

Superstrong micro-grained polycrystalline diamond compact through work hardening under high pressure

Jin Liu, Guodong Zhan, Qiang Wang, Xiaozhi Yan, Fangming Liu, Pei Wang, Li Lei, Fang Peng, Zili Kou, and Duanwei He

Citation: *Appl. Phys. Lett.* **112**, 061901 (2018);

View online: <https://doi.org/10.1063/1.5016110>

View Table of Contents: <http://aip.scitation.org/toc/apl/112/6>

Published by the [American Institute of Physics](#)



SciLight

Sharp, quick summaries **illuminating**
the latest physics research

Sign up for **FREE!**

AIP
Publishing

Superstrong micro-grained polycrystalline diamond compact through work hardening under high pressure

HPSTAR
 519-2018

Jin Liu,^{1,2,3} Guodong Zhan,^{4,a),b)} Qiang Wang,^{1,2} Xiaozhi Yan,⁵ Fangming Liu,^{1,2} Pei Wang,⁶ Li Lei,^{1,2} Fang Peng,^{1,2} Zili Kou,^{1,2} and Duanwei He^{1,2,b)}

¹Institute of Atomic and Molecular Physics, Sichuan University, Chengdu 610065, People's Republic of China

²Key Laboratory of High Energy Density Physics and Technology of Ministry of Education, Sichuan University, Chengdu 610065, People's Republic of China

³School of Mathematics and Physics, Jingchu University of Technology, Jingmen 44800, People's Republic of China

⁴College of Quality and Technical Supervision, Hebei University, Baoding 071002, People's Republic of China

⁵Center for High Pressure Science and Technology Advanced Research (HPSTAR), Shanghai 201203, People's Republic of China

⁶High Pressure Science and Engineering Center, University of Nevada, Las Vegas, Nevada 89154, USA

(Received 16 November 2017; accepted 26 January 2018; published online 6 February 2018)

We report an approach to strengthen micro-grained polycrystalline diamond (MPD) compact through work hardening under high pressure and high temperature, in which both hardness and fracture toughness are simultaneously boosted. Micro-sized diamond powders are treated without any additives under a high pressure of 14 GPa and temperatures ranging from 1000 °C to 2000 °C. It was found that the high pressure and high temperature environments could constrain the brittle feature and cause a severe plastic deformation of starting diamond grains to form a mutual bonded diamond network. The relative density is increased with temperature to nearly fully dense at 1600 °C. The Vickers hardness of the well-prepared MPD bulks at 14 GPa and 1900 °C reaches the top limit of the single crystal diamond of 120 GPa, and the near-metallic fracture toughness of the sample is as high as 18.7 MPa m^{1/2}. *Published by AIP Publishing.*

<https://doi.org/10.1063/1.5016110>

Deforming solid plastically below its recrystallization temperature, which is generally about 40% of the melting point of a metal, is known as cold plastic deformation or work hardening. The resulting metal product shows a refinement microstructure, and the known mechanisms for strengthening of metallic materials through work hardening are based on controlling defects such as dislocations to impede their motion.^{1–3} Such strategies invariably compromise ductility, the ability of the material to deform, stretch, or change its shape permanently without breaking.⁴ On the other hand, brittle materials like ordinary ceramics show no obvious ductility below their recrystallization temperatures. Thus, work hardening cannot be applied to strengthen the brittle ceramic bulks under atmospheric pressure.

Interestingly, under compression, ceramics could be deformed plastically below their recrystallization temperatures. For example, obvious plastic deformation of alumina microspheres was observed at a static pressure of ~5 GPa and 600 °C as well as at a dynamic compression of ~20 GPa and 400 °C.^{5–7} Diamond can also be yielded and exhibits plastic deformation under high pressure. Weidner *et al.* found that diamond powder started to yield under the condition of around 10 GPa and over 1000 °C.⁸ The plastic deformation of the diamond anvil surface was observed even at

room temperature and an ultra-high pressure of 220 GPa.⁹ Early in the 1970s, DeVries observed relief-polished striations and etch preferentially narrow zones in framesite which were conjectured to be the result of plastic deformation of diamond grains.¹⁰ A similar phenomenon was also found in monocrystalline diamond embedded in fine diamond powders treated at 900 °C to 1600 °C with the pressures ranging from 1 to 6 GPa,¹¹ resulting in the development of deformation lamellae defects for a significantly enhanced abrasion resistance, but the diamond particles could not be sintered into bulk materials as the pressure was not high enough. In this report, we propose that the strengthening of the micro-grained polycrystalline diamond (MPD) bulks can be achieved through the method of work hardening by inhibiting their brittle fracture under higher pressures.

The starting diamond powder (treated in a vacuum furnace at 1200 °C for 90 min) with a grain size of 8–12 μm was pressed into a pellet with a relative density of ~78%, followed by high pressure and high temperature (HPHT) treatment in a two-stage multi-anvil apparatus based on a DS6 × 25 MN cubic press machine. The pressure was estimated by the well-known pressure-induced phase transitions of Bi, ZnTe, and ZnS. The treating temperature was directly measured by using W97Re3-W75Re25 thermocouples. Samples were compressed to the desired values before heating and then treated at 1000 °C to 2000 °C under a pressure of 14 GPa.

The Vickers hardness of the end-polished samples was tested using a Vickers hardness tester (FV-700B, Future-Tech, Japan). Phase determination and structural characterization were carried out by X-ray diffraction (XRD, λCu = 1.54056 Å,

^{a)}Presently working in Drilling Technology Division, Exploration and Petroleum Engineering Center - Advanced Research Center (EXPEC-ARC), Saudi Aramco, Dhahran 31311, Saudi Arabia.

^{b)}Authors to whom correspondence should be addressed: guodong.zhan@yahoo.com and duanweihe@scu.edu.cn.

Fangyuan DX-2500, China) at $0.01^\circ/\text{s}$ steps for $2\theta = 10^\circ\text{--}100^\circ$. Raman scattering spectra were collected at room temperature in a confocal Raman system using a solid-state laser (532 nm, RGB laser system, NovaPro 300 mW, Germany) and a triple grating monochromator (Andor Shamrock SR-303i-B, EU) with an attached EMCCD (ANDOR Newton DU970P-UVB, EU). The sample morphology and microstructure were investigated by scanning electron microscopy (SEM) (FEI INSPECT F50, USA) and transmission electron microscopy (TEM) (FEI Tecnai G² F20 S-TWIN, USA).

Micro-grained diamond powder without any additives is treated at 14 GPa and different temperatures. Figure 1(a) shows the scanning electron microscopy (SEM) image of the starting diamond powder, which has an average grain size of $10\ \mu\text{m}$ with a narrow size distribution ranging from 8 to $12\ \mu\text{m}$ [Fig. 2(b)]. The choice of this grain size is mainly because the starting diamond powder for the preparation of primary commercial polycrystalline diamond materials is about $10\ \mu\text{m}$. Meanwhile, it is also convenient to characterize and observe the microstructure of the MPD samples after high pressure and high temperature treatment. The well-prepared and end-polished compacts can be prepared at over 1300°C in a form of cylinder-shaped chunks having a dimension of about 11 mm in diameter and 6 mm in thickness [Fig. 1(c)]. Those samples' dimensions are large enough for making industrial cutting/drilling tools and scientific research sampling as well.

Figure 2(a) shows the X-ray diffraction (XRD) patterns of the starting powder and MPD samples treated at different temperatures under a pressure of 14 GPa. As it can be seen, the starting grains are well-crystallized and near stress-free, which is consistent with the Raman analysis results shown in Fig. 2(b). At the treating temperature of 1500°C or above, the graphite peak appeared and became broader as temperature increased (Fig. S1, supplementary material). The relatively low stress in the triangle diamond grain boundaries (GB), the so-called Y zones, might be responsible for the graphite appearing.¹² Due to the ultra-high strength of

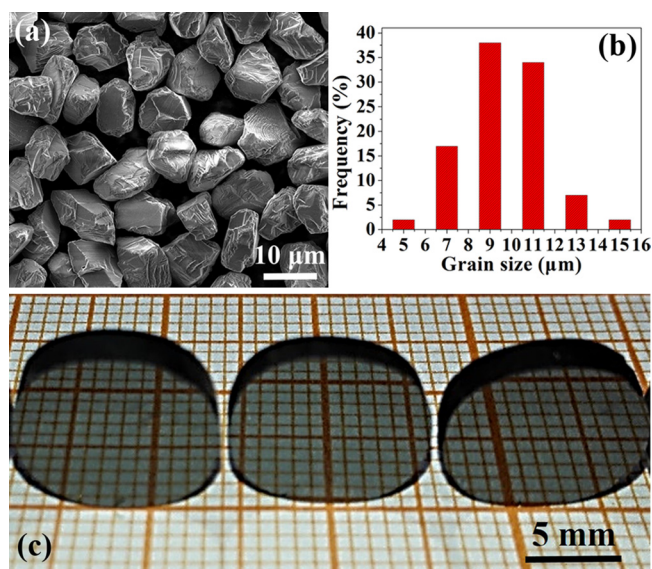


FIG. 1. (a) SEM image of starting diamond grains. (b) Statistical analysis chart of the grain size. (a) and (b) The grain size distribution of starting grains shows that the average grain size is $10\ \mu\text{m}$. (c) Optical photo of end-polished MPD samples.

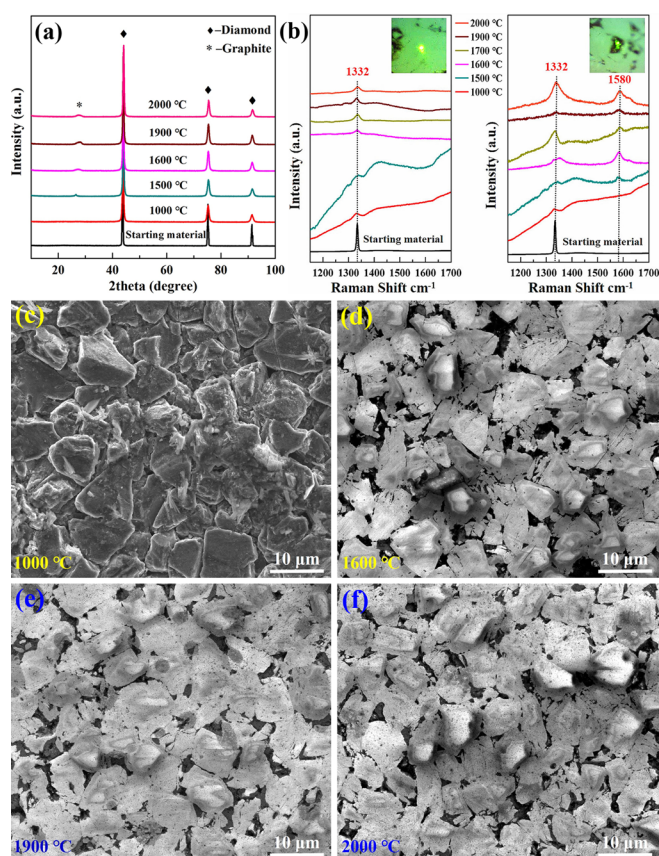


FIG. 2. (a) XRD patterns of starting grains and MPD samples. (b) Raman spectra patterns of starting grains and MPD samples. Inset: the left image represents the Raman spot projected on the bright zones of the MPD sample, and the right image (Inset) represents the dark zones (Y zones). (a) and (b) The analytical results show that the starting grains are well-crystallized, and graphitization of the diamond happened when the treating temperature went up to 1500°C . (c)–(f) SEM images of end-polished MPD samples with different treating temperatures. These images show that grain refinement and significant plastic deformation of particles appeared when treating temperature was raised up to 1600°C .

diamond, large local deviatoric/shear stress will be developed in each individual grain during the sample squeezing process.^{8,13} The strength of diamond was reported to be $\sim 15\ \text{GPa}$ at $10\ \text{GPa}$ and 1000°C ⁸ and reached as high as $130\text{--}140\ \text{GPa}$ at an ultra-high pressure of $220\ \text{GPa}$ and room temperature.⁹ Thus, the grain-to-grain contacting areas will be subjected to a relatively high stress. Conversely, the Y zones are in a state of low pressure as compared with the macroscopic pressure or average stress throughout the whole sample. As the sample temperature is increased to $\sim 1500^\circ\text{C}$, carbon atoms in the grain surface around Y zones would be out of the stable region of the diamond phase and transferred to the graphite or amorphous phase.^{14,15} However, the strength decrease of diamond with temperature rising could produce a better hydrostatic environment and lead to an actual pressure increase in the Y zones. It suggests that a further temperature increase could promote the plastic deformation of diamond and non-uniform extrusion of graphite atomic layers, as well as the graphite-to-diamond transformation. This can be reflected from the broadening and shift of graphite (200) XRD lines in Fig. 2(a).

The end-polished MPD samples' surfaces, consisting of bright zones and dark zones (Y zones) appearing under an

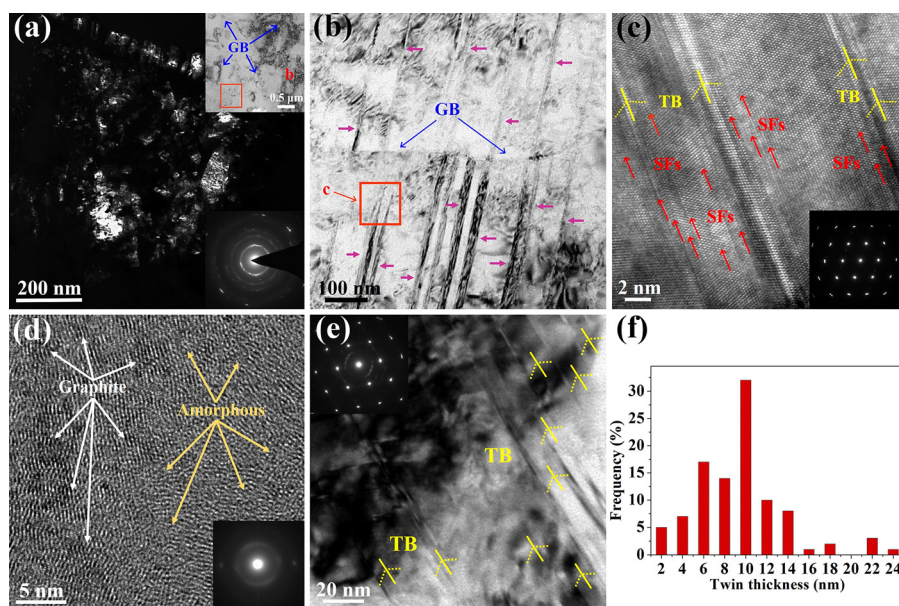


FIG. 3. Images of TEM characterization and statistical analysis chart of the average twin thickness of the MPD sample prepared at 1900 °C and 14 GPa. (a) Dark-field TEM image of the diamond grains in the Y zone of the MPD sample which is marked with the red box in the inset (up) of (a). Inset (down): the corresponding selected area electron diffraction pattern (SAED) to the area of (a). It shows that there are a large number of nano-grains in this area. (b) TEM image of densely packed dislocations marked with pink arrows in micron-sized grains which corresponds to red mark b in the inset (up) of (a). It shows that individual micro-sized diamond particle contains a large number of stacked nano-lamellae diamond and dislocations where the HRTEM image of the red box selected is shown in (c). (c) HRTEM image of the region marked with the red box in (b). Stacking faults (SFs) are marked with red arrows while twin boundaries (TB) are marked with yellow arrows. Inset: the corresponding SAED pattern of twins to the area of (c). (d) HRTEM image of turbostratic graphite and amorphous carbon in the Y zone. The white arrows represent the graphite phase and the yellow arrows represent the amorphous carbons. Inset: the corresponding SAED pattern of the amorphous carbons to the area of (d). (e) TEM image of distribution of the TB marked with yellow arrows in the grain. Inset: the corresponding SAED pattern of the twins to the area of (e). (f) Thickness distribution of the nanotwins measured from TEM and HRTEM images. The average twin thickness is 10 nm.

optical microscope, are probed using a Micro-Raman spectrometer with a laser spot diameter of $\sim 2 \mu\text{m}$ and compared to the starting powder's spectra which all are shown in Fig. 2(b). The analysis indicates that these bright regions are diamonds with a Raman peak shift of 1332 cm^{-1} for the samples treated at temperatures from 1000 °C to 2000 °C, and the signatures from dark zones are also diamond peaks at treating temperature below 1500 °C. For the samples treated at 1500 °C and above, the Micro-Raman spectrometer can probe the signatures of both diamond and graphite from the dark zones, suggesting that graphitization of the diamond happened in the Y zones during the high pressure and high temperature (HPHT) process. When temperature is increased up to 1700 °C and above, the intensity of the diamond peaks became sharper and stronger than the graphite peak compared with lower treating temperatures, suggesting that some of the graphite reconverted into diamond due to the actual pressure increasing in Y zones caused by the plastic deformation of the diamond skeleton under higher temperature conditions. Those results are consistent with the XRD analysis.

SEM images of the polished samples with different treating temperatures at 14 GPa are shown in Figs. 2(c)–2(f) and Fig. S2 (supplementary material). At low temperatures, most of the diamond grains maintain their original size and shape. Meanwhile, a large amount of broken submicron- and nano-grains are produced due to the local stress concentration at grain-to-grain contacts.^{8,12} At 1600 °C [Fig. 2(d)], the surface contact among diamond grains becomes dominant compared to that in Fig. 2(c), and the relative density of the sample reaches up to 99.2%, close to a fully dense state. As the

temperature continues increasing to 1900 °C, the diamond grains' edges become more rounded and more diamond-diamond bonding areas appear, suggesting that the rotation, rearrangement, and plastic deformation of the diamond grains are further promoted, and the Y zones are reduced as well due to the increased contacting areas of grains [Figs. 2(e), S2(d), and S2(e), supplementary material].⁸ When the treating temperature reaches 2000 °C, the diamond grains are partly sharp edged [Fig. 2(f)], and we speculate that the recrystallization of diamonds is triggered at this HPHT condition.^{14–16}

Typical transmission electron microscopy (TEM) and high resolution TEM (HRTEM) images of the MPD sample treated at 14 GPa and 1900 °C are shown in Figs. 3(a)–3(e) and S3 (supplementary material), respectively. It is found that the Y zones are composed of diamond nano-grains embedded in the turbostratic graphite and amorphous carbon [Figs. 3(a), 3(d), and S3 (supplementary material)]. Densely packed dislocations, twin boundaries (TB), and stacking faults (SFs) [seen in Figs. 3(b), 3(c), and 3(e)] are observed, which shows that each micro-sized grain contains a large amount of diamond lamellae with the thickness in the nanoscale [Fig. 3(b)]. Thickness distribution of the nanotwins measured from HRTEM images is $\sim 10 \text{ nm}$ [shown in Fig. 3(f)]. The above substructure observed in large diamond grains is a typical feature for materials after cold plastic deformation or work hardening. Similar features have also been found in the recently reported nanotwinned diamond (nt-diamond) sample synthesized from specially prepared onion carbon nanoparticles.¹⁷ Overall, the samples are composed of a diamond skeleton formed by the mutual bonding of micron-sized grains and

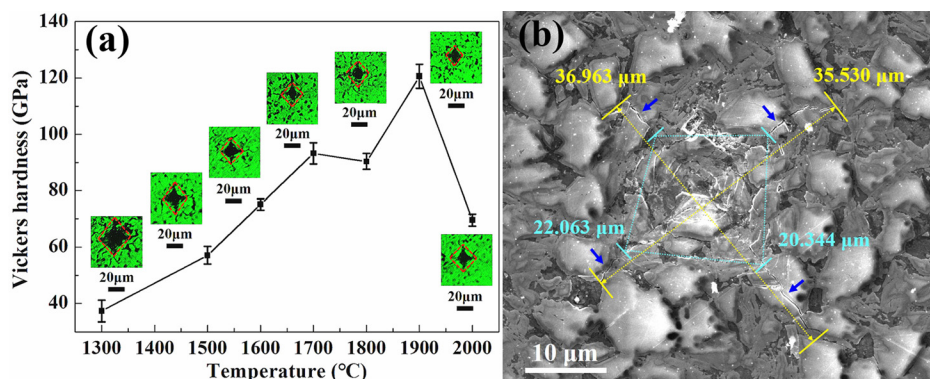


FIG. 4. (a) The relationship between Vickers hardness of MPD and different treating temperatures, and the Vickers indentations were produced with the loading force of 29.4 N and dwelling time of 15 s for the polished MPD sample. (b) SEM image of indentation and microcracks of the well-prepared MPD sample at 1900 °C and 14 GPa. The azure line segments represent the length of Vickers indentation, the yellow line segments represent the whole length of microcracks, and the blue arrows represent transgranular fracture.

isolated Y zones. Each individual micron-sized grain has a substructure of stacked nano-lamellae while the Y zone is composed of nanocrystalline diamond embedded in turbostratic graphite and amorphous carbon. This unique micro-/nano-nested structure originates from the plastic deformation of starting diamond grains and the resulting diamond-graphite reciprocal transformation during the HPHT process.

Figure 4(a) shows the Vickers hardness (H_V) results of polished MPD samples with treating temperatures from 1300 °C to 2000 °C at 14 GPa which is measured using a standard square-pyramidal diamond indenter. The loading force is 29.4 N, and the dwelling time is 15 s. The results indicate that the hardness of the samples is almost linearly increasing with the increase in the treating temperature. At the temperature of 1500 °C, the hardness is 57.1 (± 3.1) GPa, which is equivalent to the commercial polycrystalline diamond (PCD) with cobalt-based additives,^{18,19} and it increases to 120.5 (± 4.2) GPa for the 1900 °C sample, which reaches the top limit of the Vickers hardness of single crystal diamond (60–120 GPa) [Fig. 4(b) and Table SI, [supplementary material](#)].^{17,20,21} It can be seen that the hardness of the well-prepared micro-sized MPD sample is twice as high as traditional polycrystalline diamond composites and comparable to the reported nanopolycrystalline diamond (NPD) bulks (more details shown in Table SI, [supplementary material](#)).²² There are two reasons why the hardness of the samples dropped a lot when treated at 14 GPa and 2000 °C. The first reason is that the recrystallization of diamonds is triggered at this high-pressure and high-temperature condition, and as a result, the hardening effect of diamond is weakened. The second reason is that the graphitization of diamond is enhanced as the treated temperature increased to 2000 °C. This can be seen from the Raman data in the right image of Fig. 2(b) and SEM images in Figs. S2(c)–S2(f) ([supplementary material](#)).

The observed extraordinary hardness of MPD samples can be attributed to the high pressure work hardening induced nanostructured defects such as stacked nano-lamellae, stacking faults, and twinned microstructures. The defects in crystalline play a role as obstacles to dislocation glide during deformation^{22,23} and is beneficial to improving the mechanical properties. Moreover, the well-prepared MPD sample is highly grain refined, condensed, and densified in the treating process where micro-sized grains are deformed plastically to nanoscale in the substructure by squeezing among the diamond particles, leading to a further hardness enhancement due to the Hall-Petch effect.^{24,25} Quite different from conventional ways of using

graphite,²² amorphous carbon,²⁶ glassy carbon,²⁶ C₆₀,²⁶ onion-like carbon,¹⁷ or other carbons sources, our study demonstrates that the superior hardness of polycrystalline diamond materials can be achieved using the micro-sized diamond as starting materials if appropriate HPHT treatments are applied.

The fracture toughness of the MPD sample has been characterized [shown in Fig. 4(b)] and calculated by the following equation:^{27,28}

$$K_{IC} = \xi(E/H_V)^{1/2}(P/c^{3/2}) \text{ (MPa m}^{1/2}\text{)},$$

where ξ is the calibration constant of 0.0166 (± 0.004), E is the Young's modulus (GPa) (in the experiment, we used the aggregate Young's modulus, 1050 GPa, for diamond),^{8,29} P is the loading force (N), and c is the length of the crack.

The resulting K_{IC} of the prepared sample at 14 GPa and 1900 °C reaches 18.7 MPa m^{1/2}, which is about 3.7–5.5-fold of single crystal diamond (3.4–5 MPa m^{1/2}),³⁰ 7.5-fold of single crystal cBN (2.8 MPa m^{1/2}),³¹ much higher than binderless submicron cBN chunks (sm-cBN, ~ 13.2 MPa m^{1/2}),³² and superior to the reported nanotwinned cBN (nt-cBN, ~ 12.7 MPa m^{1/2}) and nanotwinned diamond (nt-diamond, ~ 9.7 to 14.8 MPa m^{1/2}).^{17,20} At the same time, as shown in Fig. 4(b) (marked with blue arrows), it is very interesting to note that microcracks are mainly produced on diamond micro-grains and terminated at the grain boundaries (Y zones). The nanostructured Y zones consisting of nanocrystalline diamond grains, turbostratic graphite, and amorphous carbon can significantly stop the cracks from further propagation and thus greatly improve the fracture toughness of the prepared sample.

In conclusion, superstrong micro-grained polycrystalline diamond compacts have been prepared through work hardening at high pressure. The high pressure and high temperature environments could constrain the brittle feature and cause a severe plastic deformation of starting diamond grains to form a mutual bonded diamond network together with isolated Y zones. Both the diamond skeleton and Y zone are in the micro-scale while having a nanostructure inside, and this unique micro-/nano-nested microstructure makes the material extremely strong in terms of both hardness and fracture toughness. We believe that the proposed and demonstrated high pressure work hardening approach can be applied to other brittle materials to inhibit their brittle fracturing for enhancing their mechanical properties for a wide range of applications.

See [supplementary material](#) for more details on sample preparation and characterization results using XRD, SEM, and TEM methods for starting material and samples prepared at different conditions. More information is given on various superhard materials with different preparation methods and their mechanical properties.

This work was supported by the National Natural Science Foundation of China (Grant Nos. 51472171, 11427810, and 11704014) and the project for the Science and Technology Innovation Team of Sichuan Province (Grant No. 15CXTD0025). We also thank Alex S. Zhan (the University of Texas at Austin) for careful reading of the manuscript.

- ¹R. W. Armstrong, I. Codd, R. M. Douthwaite, and N. J. Petch, *Philos. Mag.* **7**, 45 (1962).
- ²T. Sakai, A. Belyakov, R. Kaibyshev, H. Miura, and J. J. Jonas, *Prog. Mater. Sci.* **60**, 130 (2014).
- ³T. Saito, T. Furuta, J. H. Hwang, S. Kuramoto, K. Nishino, N. Suzuki, and T. Nonaka, *Science* **300**, 464 (2003).
- ⁴K. Lu, L. Lu, and S. Suresh, *Science* **324**, 349 (2009).
- ⁵F. Liu, D. He, P. Liu, H. Wang, C. Xu, S. Yin, W. Yin, and Y. Li, *J. Appl. Phys.* **114**, 233504 (2013).
- ⁶F. Liu, D. He, Q. Wang, W. Ding, J. Liu, and Y. Liu, *Scr. Mater.* **122**, 54 (2016).
- ⁷E. K. Beauchamp, M. J. Carr, and R. A. Graham, *J. Am. Ceram. Soc.* **68**, 696 (1985).
- ⁸D. J. Weidner, Y. Wang, and M. T. Vaughan, *Science* **266**, 419 (1994).
- ⁹M. I. Eremets, I. A. Trojan, P. Gwaze, J. Huth, R. Boehler, and V. D. Blank, *Appl. Phys. Lett.* **87**, 141902 (2005).
- ¹⁰R. C. DeVries, *Mater. Res. Bull.* **8**, 733 (1973).
- ¹¹R. C. DeVries, *Mater. Res. Bull.* **10**, 1193 (1975).
- ¹²J. Wang, D. He, and T. S. Duffy, *J. Appl. Phys.* **108**, 063521 (2010).
- ¹³D. He, S. R. Shieh, and T. S. Duffy, *Phys. Rev. B* **70**, 184121 (2004).
- ¹⁴L. M. Ghiringhelli, J. H. Los, E. J. Meijer, A. Fasolino, and D. Frenkel, *Phys. Rev. Lett.* **94**, 145701 (2005).
- ¹⁵C. Xu, D. He, H. Wang, J. Guan, C. Liu, F. Peng, W. Wang, Z. Kou, K. He, X. Yan, Y. Bi, L. Liu, F. Liu, and B. Hui, *Int. J. Refract. Met. Hard Mater.* **36**, 232 (2013).
- ¹⁶F. P. Bundy, *J. Chem. Phys.* **38**, 631 (1963).
- ¹⁷Q. Huang, D. Yu, B. Xu, W. Hu, Y. Ma, Y. Wang, Z. Zhao, B. Wen, J. He, Z. Liu, and Y. Tian, *Nature* **510**, 250 (2014).
- ¹⁸S. M. Hong, M. Akashi, and S. Yamaoka, *J. Am. Ceram. Soc.* **82**, 2497 (1999).
- ¹⁹Z. J. Lin, J. Z. Zhang, B. S. Li, L. P. Wang, H.-K. Mao, R. J. Hemley, and Y. Zhao, *Appl. Phys. Lett.* **98**, 121914 (2011).
- ²⁰Y. Tian, B. Xu, D. Yu, Y. Ma, Y. Wang, Y. Jiang, W. Hu, C. Tang, Y. Gao, K. Luo, Z. Zhao, L. Wang, B. Wen, J. He, and Z. Liu, *Nature* **493**, 385 (2013).
- ²¹C. S. Yan, H. K. Mao, W. Li, J. Qian, Y. Zhao, and R. J. Hemley, *Phys. Status Solidi A* **201**, R25 (2004).
- ²²T. Irifune, A. Kurio, S. Sakamoto, T. Inoue, and H. Sumiya, *Nature* **421**, 599 (2003).
- ²³G. D. Zhan, J. D. Kuntz, J. Wan, and A. K. Mukherjee, *Nat. Mater.* **2**, 38 (2003).
- ²⁴E. O. Hall, *Proc. Phys. Soc., London, Sect. B* **64**, 747 (1951).
- ²⁵N. J. Petch, *J. Iron Steel Inst.* **174**, 25 (1953).
- ²⁶H. Sumiya and T. Irifune, *J. Mater. Res.* **22**, 2345 (2007).
- ²⁷G. R. Anstis, P. Chantikul, B. R. Lawn, and D. B. Marshall, *J. Am. Ceram. Soc.* **64**, 533 (1981).
- ²⁸A. G. Evans and E. A. Charles, *J. Am. Ceram. Soc.* **59**, 371 (1976).
- ²⁹M. H. Grimsditch and A. K. Ramdas, *Phys. Rev. B* **11**, 3139 (1975).
- ³⁰N. Dubrovinskaia, S. Dub, and L. Dubrovinsky, *Nano Lett.* **6**, 824 (2006).
- ³¹V. L. Solozhenko, O. O. Kurakevych, and Y. L. Godec, *Adv. Mater.* **24**, 1540 (2012).
- ³²G. Liu, Z. Kou, X. Yan, L. Lei, F. Peng, Q. Wang, K. Wang, P. Wang, L. Li, Y. Li, W. Li, Y. Wang, Y. Bi, Y. Leng, and D. He, *Appl. Phys. Lett.* **106**, 121901 (2015).